PNAS RESEARCH ARTICLE | MEDICAL SCIENCES

Targeting DTX2/UFD1-mediated FTO degradation to regulate antitumor immunity

Yan-Hong Cui[a], Jiangbo Wei[b,c], Hao Fan[d], Wenlong Li[b,c], Lijie Zhao[b,c], Emma Wilkinson[a,e], Jack Peterson[a,f], Lishi Xie[d], Zhongyu Zou[b,c], Seungwon Yang[a], Mark A. Applebaum[g], Justin Kline[d], Jing Chen[d], Chuan He[b,c,h], and Yu-Ying He[a,1]

Affiliations are included on p. 11.

Edited by Myles Brown, Dana-Farber Cancer Institute, Boston, MA; received April 19, 2024; accepted November 11, 2024

Here, we show that vitamin E succinate (VES) acts as a degrader for the m^{6}A RNA demethylase fat mass and obesity-associated protein (FTO), thus suppressing tumor growth and resistance to immunotherapy. FTO is ubiquitinated by its E3 ligase DTX2, followed by UFD1 recruitment and subsequent degradation in the proteasome. VES binds to FTO and DTX2, leading to enhanced FTO–DTX2 interaction, FTO ubiquitination, and degradation in FTO-dependent tumor cells. VES suppressed tumor growth and enhanced antitumor immunity and response to immunotherapy in vivo in mouse models. Genetic FTO knockdown or VES treatment increased m^{6}A methylation in the LIF (Leukemia Inhibitory Factor) gene and decreased LIF mRNA decay, and thus sensitized melanoma cells to T cell–mediated cytotoxicity. Taken together, our findings reveal the underlying molecular mechanism for FTO protein degradation and identify a dietary degrader for FTO that inhibits tumor growth and overcomes immunotherapy resistance.

FTO | m^{6}A RNA methylation | DTX2 | ubiquitin-mediated proteasomal degradation | UFD1

N^6-methyladenosine (m^{6}A) methylation in RNA has been considered the most abundant posttranscriptional RNA modification in eukaryote mRNA and plays critical roles in almost all RNA metabolism processes (1–5). Recent studies have shown that m^{6}A RNA modification has vital roles in various physiological and pathological processes, especially in different types of cancers (6–8). As the first m^{6}A RNA demethylase identified (9), FTO belongs to the nonheme Fe(II)- and α-ketoglutarate (αKG)-dependent AlkB dioxygenase family of proteins (10, 11). Emerging evidence has demonstrated a critical role for FTO in development and diseases (12). In particular, FTO has been reported to be up-regulated and to act as a tumor-promoting factor in multiple types of cancers (4, 8, 13). Consequently, several small-molecule inhibitors for FTO have been identified, including Rhein, MA, FB23/23-2, R-2HG, CS1/2, and Dac51 (14–25). Among these FTO inhibitors, several have shown promising therapeutic effects in preclinical mouse tumor models (21–23, 25). However, despite the identification of these small-molecule FTO inhibitors, most toxicology profiles are either unknown or undesirable, limiting their translation potentials into the clinic.

Protein degradation is a ubiquitous cellular process that controls protein homeostasis and plays critical roles in numerous cellular processes (26). One protein degradation system is the ubiquitin–proteasome pathway. Excessive, damaged, or misfolded proteins are ubiquitinated and ultimately delivered to the proteasome for degradation. Ubiquitination is governed by the sequential activity of ubiquitin-activating enzymes (E1s), ubiquitin-conjugating enzymes (E2s), and ubiquitin ligases (E3s) that sequentially activate, conjugate, and ligate ubiquitin to protein substrate targets (27). E3 ubiquitin ligases determine the substrate specificity of ubiquitination and play essential roles in the intricate cell signaling networks (28). There are about 600 human E3 ligases currently identified. The understanding of the molecular machinery controlling protein degradation has led to the development of heterobifunctional protein degraders, such as PROteolysis Targeting Chimera (PROTAC) protein degraders, as a new therapeutic modality (29). Ten E3 ligases have been exploited for targeted protein degradation (TPD), including cereblon (CRBN), von Hippel–Lindau tumor suppressor (VHL), and MDM2 (30). The teratogenic agent thalidomide and its derivatives have been discovered to possess anticancer activity via targeted protein degradation and became FDA-approved PROTAC agents to treat hematological malignancies and Kaposi sarcoma (31). As compared with small-molecule enzymatic inhibitors, protein degraders eliminate proteins rather than inhibiting protein activity and thus offer several advantages including their event-driven (rather than occupancy-driven) pharmacology, their capability to target multiple copies of a target

Significance

The m^{6}A RNA demethylase fat mass and obesity-associated protein (FTO) is aberrantly up-regulated in numerous cancers. Here, we report that vitamin E succinate (VES), a widely used dietary supplement and a vitamin E derivative, acts as a degrader for FTO. VES interacts with both FTO and its E3 ligase DTX2, leading to increased FTO ubiquitination and degradation. FTO depletion genetically or by VES increased tumor-intrinsic immune response and T cell cytotoxicity, decreased tumor growth, and sensitized tumors to immunotherapy. Our work on FTO degradation mechanisms and VES as a degrader may provide a mechanistic foundation and framework for the development of better degraders for FTO with improved potency and specificity for cancer intervention and therapy.

Author contributions: Y.-H.C., J.W., H.F., J.C., C.H., and Y.-Y.H. designed research; Y.-H.C., J.W., and H.F. performed research; Y.-H.C., L.Z., L.X., S.Y., and J.K. contributed new reagents/analytic tools; Y.-H.C., J.W., H.F., W.L., L.Z., E.W., J.P., Z.Z., and M.A.A. analyzed data; Z.Z. participated in discussions; and Y.-H.C. and Y.-Y.H. wrote the paper.

Competing interest statement: C.H. is a scientific founder and a scientific advisory board member of Accent Therapeutics, Inc., Inferna Green, Inc., and AccuaDX, Inc. The remaining authors declare no competing interests.

This article is a PNAS Direct Submission.

[1]To whom correspondence may be addressed. Email: yyhe@bsd.uchicago.edu.

This article contains supporting information online at https://www.pnas.org/lookup/suppl/doi:10.1073/pnas.2407910121/-/DCSupplemental.

Published December 11, 2024.

protein, and their potential to target nonenzymatic proteins or those traditionally considered undruggable (29, 31).

Our previous work has demonstrated that FTO is ubiquitinated and stabilized by chronic low-level arsenic exposure (32). However, how FTO ubiquitination and degradation are executed and regulated are not known. This knowledge gap has hindered the development of FTO degraders that can potentially be utilized in therapies against FTO-dependent cancers and other diseases. In this study, we have identified DTX2 as an E3 ubiquitin ligase for FTO and UFD1 as a ubiquitinated-FTO-binding protein, leading to FTO degradation. Our data uncovered that alpha-tocopherol succinate, also known as vitamin E succinate (VES), a vitamin E derivative, acts as a FTO degrader to suppress tumorigenesis and enhance antitumor immunity and tumor response to immunotherapy in mouse models.

Results

DTX2 Is an E3 Ubiquitin Ligase for FTO that Induces FTO Ubiquitination and Degradation. We propose that FTO protein stability may be regulated and play an important role in cancer development. Supporting this hypothesis, we found that a high FTO protein level is associated with poor survival in breast cancer (*SI Appendix*, Fig. S1*A*), while such an association was not detected between the FTO mRNA level and survival (*SI Appendix*, Fig. S1*B*). Moreover, the FTO protein level did not show a pattern similar to its mRNA level in different melanoma cell lines (*SI Appendix*, Fig. S1 *C* and *D*), suggesting that FTO can be regulated at the protein level in melanoma. Additionally, we observed that UVB irradiation, a major environmental carcinogen for skin cancer, including melanoma, increases FTO protein stability (*SI Appendix*, Fig. S1 *E* and *F*). Furthermore, the FTO protein level was increased and the m^6A level was decreased in WM35 melanoma cells after treatment with the supernatant from UVB-irradiated keratinocytes (*SI Appendix*, Fig. S1 *G* and *H*), while it had no effect on FTO mRNA levels (*SI Appendix*, Fig. S1*I*). Taken together, these findings suggest a role for protein degradation in regulating FTO protein expression in carcinogenesis.

To determine the molecular mechanism of regulating FTO protein stability, using the Protein Interaction Network Analysis (PINA) platform (33–35), we first assessed whether FTO-interacting proteins (*SI Appendix*, Fig. S2 *A–C*) may play a role in FTO degradation. Among these proteins, we focused on enzymes involved in protein ubiquitination and cancer. The expression of RECQL4, DTX2, BCCIP, or MAD2L2 was negatively associated with FTO expression, while the expression of NPEPPS, SBF2, CLUAP1, ZMAT3, or ANKRD11 was positively correlated with FTO expression (*SI Appendix*, Fig. S2 *A* and *B*). We elected to focus on DTX2, as it is an E3 ubiquitin ligase that regulates protein degradation (36). Indeed, DTX2 expression was negatively correlated with FTO expression in Pan-cancer patient data (*SI Appendix*, Fig. S2 *D* and *E*).

Next, we investigated whether DTX2 acts as an E3 ligase for FTO to regulate FTO protein degradation. First, we found that DTX2 knockdown increases FTO protein level but not its mRNA level (*SI Appendix*, Fig. S3 *A* and *B*), while DTX2 overexpression decreases FTO protein level (*SI Appendix*, Fig. S3 *C* and *D*). Consistently, DTX2 knockdown increased the expression of CXCR4 (*SI Appendix*, Fig. S3*E*), an FTO target gene in melanoma (37). The proteasome inhibitor MG132 inhibited a DTX2-induced drastic decrease in FTO protein level (Fig. 1*A* and *SI Appendix*, Fig. S3*F*). Additionally, DTX2 overexpression drastically reduced FTO protein stability (Fig. 1 *B* and *C* and *SI Appendix*, Fig. S3 *G* and *H*). Coimmunoprecipitation (Co-IP) analysis showed that DTX2 binds to FTO (*SI Appendix*, Fig. S3*I*).

To determine the domain of DTX2 responsible for its binding with FTO, we generated DTX2 mutants with deletion of DTX2's functional domains WWE1, WWE2, and RING (36, 38) (Fig. 1*D*). Wild-type (WT) but not mutant DTX2 (WWE1, WWE2, and RING) decreased the FTO protein level (*SI Appendix*, Fig. S3*J*). As compared with WT DTX2, mutant DTX2 showed reduced binding with FTO (Fig. 1*E* and *SI Appendix*, Fig. S3*K*). Furthermore, DTX2 knockdown decreased FTO ubiquitination (*SI Appendix*, Fig. S3*L*), while overexpression of WT DTX2 increased FTO ubiquitination (Fig. 1*F*). However, as compared with WT DTX2, DTX2 mutants with deletion of the WWE1, WWE2, or RING domain resulted in decreased FTO ubiquitination (Fig. 1*F*), implicating that these DTX2 domains are critical for FTO ubiquitination. Furthermore, we confirmed that DTX2 overexpression reverses the effect of FTO on m^6A enrichment (Fig. 1*G*).

Lysine ubiquitination is one of the most abundant posttranslational modifications (PTMs) in the human proteome. RING-domain E3 ligases mediate the transfer of ubiquitin to the substrate lysine (39, 40). To determine the lysine site in FTO targeted for ubiquitination, we searched the lysine ubiquitination sites of FTO from the PhosphoSitePlus® website and found that most lysines are located in the N terminus of FTO (*SI Appendix*, Fig. S3*M*). The structure of FTO consists of N-terminal domains (NTD) and C-terminal domains (CTD); the NTD controls core catalytic activity with the involvement of the CTD (41). We elected to initially focus on the lysines close to the C terminus (K121–K216) in FTO and generated K-to-R mutants for these lysines. Indeed, all mutants showed drastically increased FTO protein levels (Fig. 1*H*) and decreased m^6A levels (Fig. 1*I*). FTO lysine mutants, including K160R, K162R, K194R, and K216R, increased FTO protein stability (Fig. 1 *J* and *K* and *SI Appendix*, Fig. S3 *N* and *O*). Consistently, these lysine mutants showed higher FTO abundance as compared with WT FTO and prevented DTX2-mediated FTO downregulation (Fig. 1*L* and *SI Appendix*, Fig. S3*P*), suggesting that all of these lysine residues are critical for DTX2-mediated FTO degradation. In particular, the K162R mutant showed the lowest m^6A level as compared with WT FTO and other lysine mutants (Fig. 1*I*). Consistently, K162R FTO abundance and stability was higher than WT FTO (*SI Appendix*, Fig. S3*Q*) and prevented the effect of DTX2 overexpression on FTO degradation (*SI Appendix*, Fig. S3*R*) and ubiquitination (Fig. 1*M*). To determine which ubiquitin chain is critical for DTX2-mediated FTO ubiquitination and degradation, we assessed the role of the ubiquitin chain assembled via lysine 48 (K48), a primary targeting signal for proteasomal recognition and degradation of polyubiquitinated proteins (42). Indeed, the K48R ubiquitin mutant drastically reduced DTX2-mediated FTO ubiquitination, suggesting K48-linked polyubiquitination as the major ubiquitin chain for FTO (Fig. 1*N*). Taken together, these data demonstrate that DTX2 acts as an E3 ligase for FTO.

VES Induces FTO Protein Degradation. Next, we elected to identify dietary FTO degraders that can knock down FTO protein chemically and can be taken as a supplement for cancer prevention, interception, or therapy. We focused on vitamins, which are widely used dietary supplements. Recent work has demonstrated that vitamins C and E enhance the response to immunotherapy (43–45). Among the different vitamin E derivatives investigated previously, VES seems to possess a notable anticancer effect in vitro and in vivo (46–49). In particular, the succinate moiety in VES is structurally similar to αKG, the cosubstrate for FTO to catalyze the oxidative demethylation of N-methylated RNA/DNA substrates (10, 50). In addition, succinate and succinate derivatives have been shown to inhibit FTO activity (10, 50).

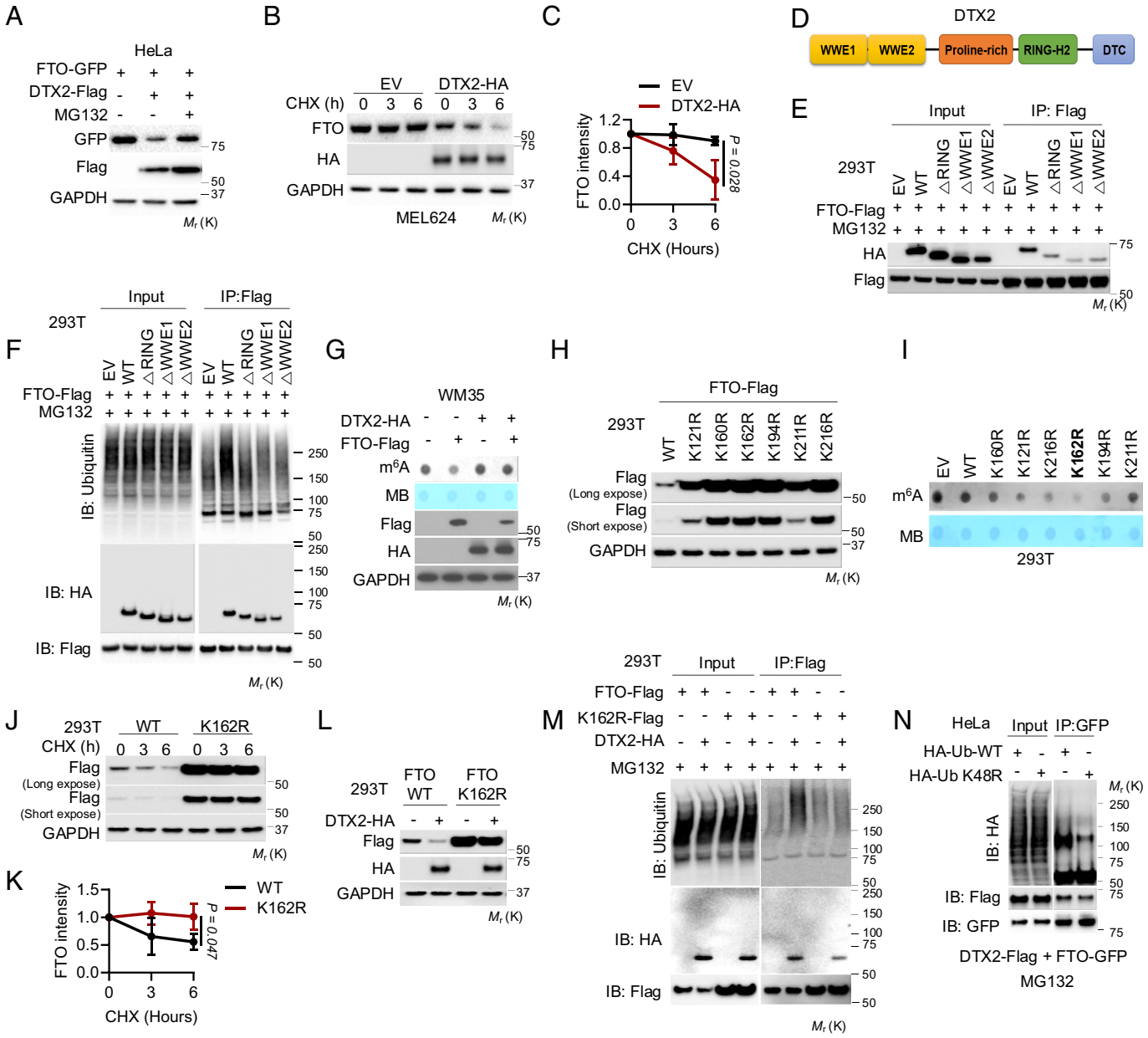

Fig. 1. DTX2 is an E3 ubiquitin ligase for FTO that induces FTO ubiquitination and degradation. (*A*) Immunoblot analysis of FTO-GFP and DTX2-Flag in FTO-GFP-overexpressed HeLa cells with or without overexpression of DTX2-Flag treated with or without MG132 (10 μM) for 6 h. GAPDH was used as a loading control. (*B*) Immunoblot analysis of FTO in MEL624 cells transfected with empty vector (EV) or DTX2-HA treated with cycloheximide (CHX, 100 μg/ml) over a time course. (*C*) Quantification of *B* (n =3). (*D*) Domain architecture of human DTX2. (*E*) Coimmunoprecipitation (Co-IP) assay of FTO binding with HA-tagged wild-type (WT) DTX2 or DTX2 mutants with deletions of domains in 293T cells transfected with Empty Vector (EV), △RING-HA, △WWE1-HA, △WWE2-HA, in combination with FTO-Flag and treated with MG132 (10uM) for 6 h. (*F*) Ubiquitination assay of 293T cells transfected with constructs expressing FTO-Flag, and WT DTX2-HA or DTX2 mutants and treated with MG132 (10 μM) for 6 h. Protein lysates were immunoprecipitated with the Flag-beads and ubiquitination was detected with the anti-Ubiquitin antibody. (*G*) m^6A dot blot assay and immunoblot analysis in WM35 cells transfected with or without DTX2-HA and FTO-Flag. (*H*) Immunoblot analysis of FTO-Flag and FTO-Flag mutants with indicated arginine mutation in Lysine (K121R, K160R, K162R, K194R, K211R, and K216R) in 293T cells transfected WT and FTO lysine mutants. (*I*) m^6A dot blot assay in 293T cells transfected with WT and FTO lysine mutants. (*J*) Immunoblot analysis of WT and FTO K162R in 293T cells transfected with WT and FTO K162R and treated with cycloheximide (CHX, 100 μg/ml) over a time course. (*K*) Quantification of J (n = 3). (*L*) Immunoblot analysis of Flag for WT and K162R FTO, and HA (DTX2) in 293T cells transfected with or without DTX2 in combination with FTO WT or K162R. (*M*) Ubiquitination assay of 293T cells transfected with or without constructs expressing DTX2-HA, FTO WT-Flag, and K162R-Flag and treated with MG132 (10 μM) for 6 h. Protein lysates were immunoprecipitated with the Flag-beads and ubiquitination was detected with the anti-Ubiquitin antibody. (*N*) Ubiquitination assay of HeLa cells transfected with or without HA-Ub WT or HA-Ub K48R in combination with DTX2-Flag or FTO-GFP and then treated with MG132 (10 μM) for 6 h. Protein lysates were immunoprecipitated with the anti-GFP antibody and ubiquitination was detected with the anti-HA antibody. Error bars are shown as mean ± SD (*C* and *K*). *P*-values are from two-tailed unpaired *t* test (*C* and *K*).

Thus, we questioned whether VES binds to FTO via the succinate moiety and thus regulates FTO stability or activity.

Indeed, as compared with succinate (dimethyl succinate, DS), vitamin E (VE), and vitamin E acetate (VEA), VES drastically inhibited cell proliferation (*SI Appendix*, Fig. S4*A*) and decreased the FTO protein level (*SI Appendix*, Fig. S4*B*). Mimicking FTO knockdown (*SI Appendix*, Fig. S4*C*), VES increased m^6A enrichment (Fig. 2*A* and *SI Appendix*, Fig. S4*D*). Cellular thermal shift assay (CETSA) and drug affinity responsive target stability (DARTS) analyses suggested that VES binds with FTO (Fig. 2 *B* and *E* and *SI Appendix*, Fig. S4 *E* and *F*). To determine how VES binds with FTO, we used molecular

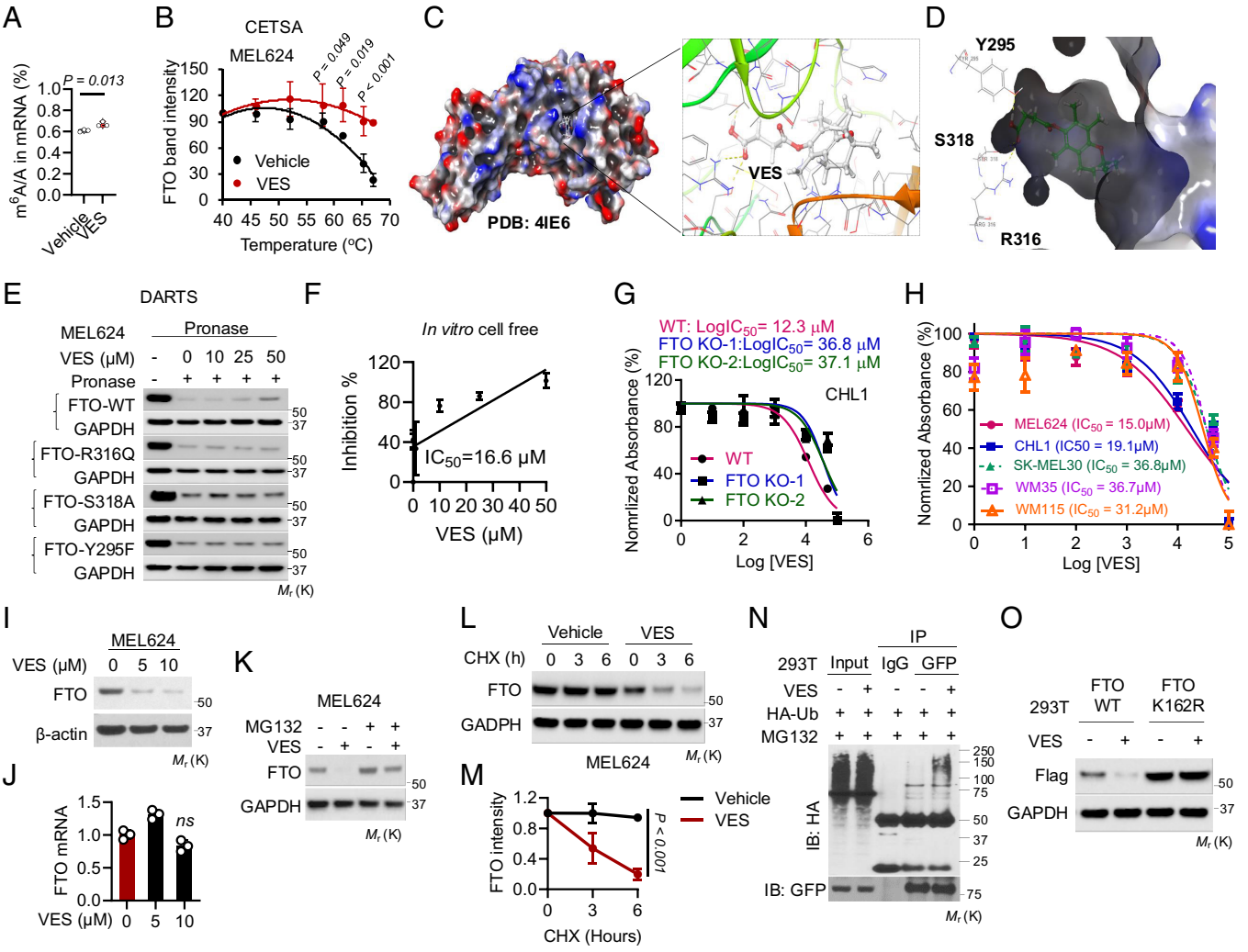

Fig. 2. VES induces FTO protein degradation. (*A*) Quantification of the m^{6}A/A ratios in mRNA by LC-MS/MS in MEL624 cells with or without VES treatment (n = 3). (*B*) Thermal shift curves of FTO from CETSA in MEL624 cells treated with or without VES (10 μM) (n = 3). (*C*) Molecular docking models for the interaction between human FTO (PDB: 4IE6) and VES without the aliphatic chain using Schrodinger. (*D*) Model for FTO binding with VES without the aliphatic chain. (*E*) Immunoblot analysis of WT and FTO mutants (R316Q, S318A, and Y295F) from the DARTS assay in MEL624 cells treated with or without VES. (*F*) Inhibitory effects of VES on FTO demethylase activity using an in vitro (cell-free) m^{6}A demethylation assay. (*G*) IC50 values of VES (72 h) on inhibiting cell viability in CHL1 cells with or without FTO knockout (KO) (n = 3). (*H*) IC50 values of VES (72 h) on inhibiting cell viability in FTO-high melanoma cell lines (MEL624, CHL1) and FTO-low melanoma cell lines (SK-MEL-30. WM35, WM115) (n = 3). (*I*) Immunoblot analysis of FTO in MEL624 cells treated with VES at indicated doses. β-actin was used as a loading control. (*J*) qPCR analysis of FTO mRNA levels in cells as in I (n = 3). (*K*) Immunoblot analysis of FTO in MEL624 cells with or without VES (10 μM, 72 h) and MG132 (10 μM) added for 6 h prior to the end of 72 h. (*L*) Immunoblot analysis of FTO in MEL624 cells treated with or without VES (10 μM, 72 h) and then cycloheximide (CHX, 100 μg/ml) over a time course. (*M*) Quantification of *L* (n = 3). (*N*) Ubiquitination assay of 293T cells transfected with HA-Ub and FTO-GFP and treated with or without VES (25 μM, 12 h) and/or MG132 (10 μM, 6 h). Protein lysates were immunoprecipitated with the anti-GFP antibody and ubiquitination was detected with the anti-HA antibody. (*O*) Immunoblot analysis of WT and K162R FTO in 293T cells transfected with Flag-tagged WT FTO and FTO K162R and treated with or without VES (25 μM, 72 h). Error bars are shown as mean ± SE (*F*) and ± SD (*A*, *B*, *G*, *H*, *J*, and *M*). *P*-values are from two-tailed unpaired *t* tests (*A*, *B*, *J*, and *M*).

docking to identify the potential binding sites (Fig. 2*C* and *SI Appendix*, Fig. S4*G*). We found that VES binds with FTO at the R316, S318, and Y295 residues (Fig. 2*D* and *SI Appendix*, Fig. S4*H*). To assess the importance of these residues in VES-FTO binding, we generated R316Q, S318A, and Y295F FTO mutants. DARTS analysis showed that all three FTO mutants fail to bind with VES (Fig. 2*E*). To confirm whether VES interacts with FTO and modulates FTO activity, we performed an in vitro cell-free assay of m^{6}A demethylase activity of recombinant FTO protein. We found that VES inhibits the m^{6}A demethylase activity of FTO (Fig. 2*F*). These findings implicate that VES interacts with FTO and reduces FTO's m^{6}A demethylase activity.

To determine whether FTO is a selective target for VES, we generated FTO knockout (KO) cells using CRISPR. FTO deletion reduced the sensitivity to VES (Fig. 2*G* and *SI Appendix*, Fig. S5*A*). Similarly, melanoma cell lines with low FTO expression (SK-MEL30, WM35, and WM115) showed reduced sensitivity to VES as compared with those with high FTO expression (CHL1 and MEL624) (Fig. 2*H*). Previous data showed that VES has proapoptotic properties in multiple hematopoietic and carcinoma cell lines (46–49, 51). Interestingly, we found that VES induces apoptosis at a high dose (25 μM), but not lower doses (*SI Appendix*, Fig. S5*B*). Moreover, VES at lower doses (5 and 10 μM) drastically decreased FTO protein levels (Fig. 2*I* and *SI Appendix*, Fig. S5 *B* and *C*) without affecting FTO mRNA level (Fig. 2*J* and *SI Appendix*, Fig. S5*D*), suggesting that VES's effect on FTO is not due to cell death. VES increased m^{6}A enrichment and decreased expression of the FTO target genes CXCR4, SOX10, and PDCD1, resembling the effect of FTO genetic inhibition (*SI Appendix*, Fig. S5 *E*–*I*).

Targeted protein degradation (TPD) is an emerging therapeutic modality that has expanded the druggable proteome for cancer treatment (52). We hypothesized that VES interacts with FTO and acts as an FTO degrader. Indeed, the proteasome inhibitor MG132 increased FTO protein level (*SI Appendix*, Fig. S5 *J* and *K*) and reversed the effect of VES (Fig. 2*K*). Furthermore, VES decreased protein stability (Fig. 2 *L* and *M* and *SI Appendix*, Fig. S5 *L* and *M*) and increased ubiquitination of WT FTO (Fig. 2*N*), while it had no effect on the FTO K162R mutant (Fig. 2*O*). Next, we assessed whether VES affects FTO protein levels specifically, but not the levels of other αKG-dependent dioxygenases, including enzymes involved in methylation of DNA and histones, or other m^6A regulators. We found that VES has little or no effect on the protein levels of these enzymes, histone modifications, or 5-hmC DNA demethylation (*SI Appendix*, Fig. S5 *N* and *O*). In addition, VES did not affect the level of the m^6A methyltransferase proteins METTL3 and METTL14 (*SI Appendix*, Fig. S5*P*). Moreover, cells with FTO deletion were resistant to VES's effect on m^6A enrichment (*SI Appendix*, Fig. S5*Q*). Furthermore, inhibition of METTL3 reduced the basal m^6A levels, while it failed to restore the effect of VES in FTO KO cells (*SI Appendix*, Fig. S5*Q*) or affect proliferation in CHL1 cells with FTO deletion (*SI Appendix*, Fig. S5*R*), suggesting that FTO, but not METTL3, is the target of VES. Taken together, these findings demonstrate that VES is a selective FTO degrader.

VES Induces FTO Protein Degradation Via DTX2. Next, we assessed the role of DTX2 in VES-induced FTO degradation. An in situ proximity ligation assay (PLA) assay showed that VES increases FTO–DTX2 interaction (Fig. 3 *A*–*C*). In addition, Co-IP analysis showed that VES increased FTO binding with DTX2 (Fig. 3*D*). Moreover, DTX2 knockdown reversed the effect of VES on FTO protein degradation (Fig. 3*E*). Next, we questioned whether the vitamin E moiety of VES binds with DTX2, because the succinate moiety of VES binds with FTO (Fig. 2 *F* and *G* and *SI Appendix*, Fig. S4 *G* and *H*). As expected, molecular docking analysis showed that vitamin E binds with DTX2 (Fig. 3 *F* and *G*). DARTS analysis showed that VES and VE, but not succinate, bind with DTX2 (Fig. 3*H*). Next, we assessed whether the effect of VES is specific for FTO. DTX2 overexpression decreased the protein level of FTO, while it had no effect on the protein level of ALKBH5, another m^6A RNA demethylase and member of the Fe^{2+}- and 2-oxoglutarate (2OG)-dependent AlkB dioxygenase family (*SI Appendix*, Fig. S5*O* and S6*A*). In addition, DTX2 did not bind with ALKBH5; and DTX2 expression was not negatively correlated with ALKBH5 expression in cancers (*SI Appendix*, Fig. S6 *B* and *C*). Furthermore, published small molecular FTO inhibitors CS1, CS2, and FB23-2 had either no effect or less effect on FTO protein inhibition than VES (*SI Appendix*, Fig. S6*D*). Taken together, these results implicate that VES acts

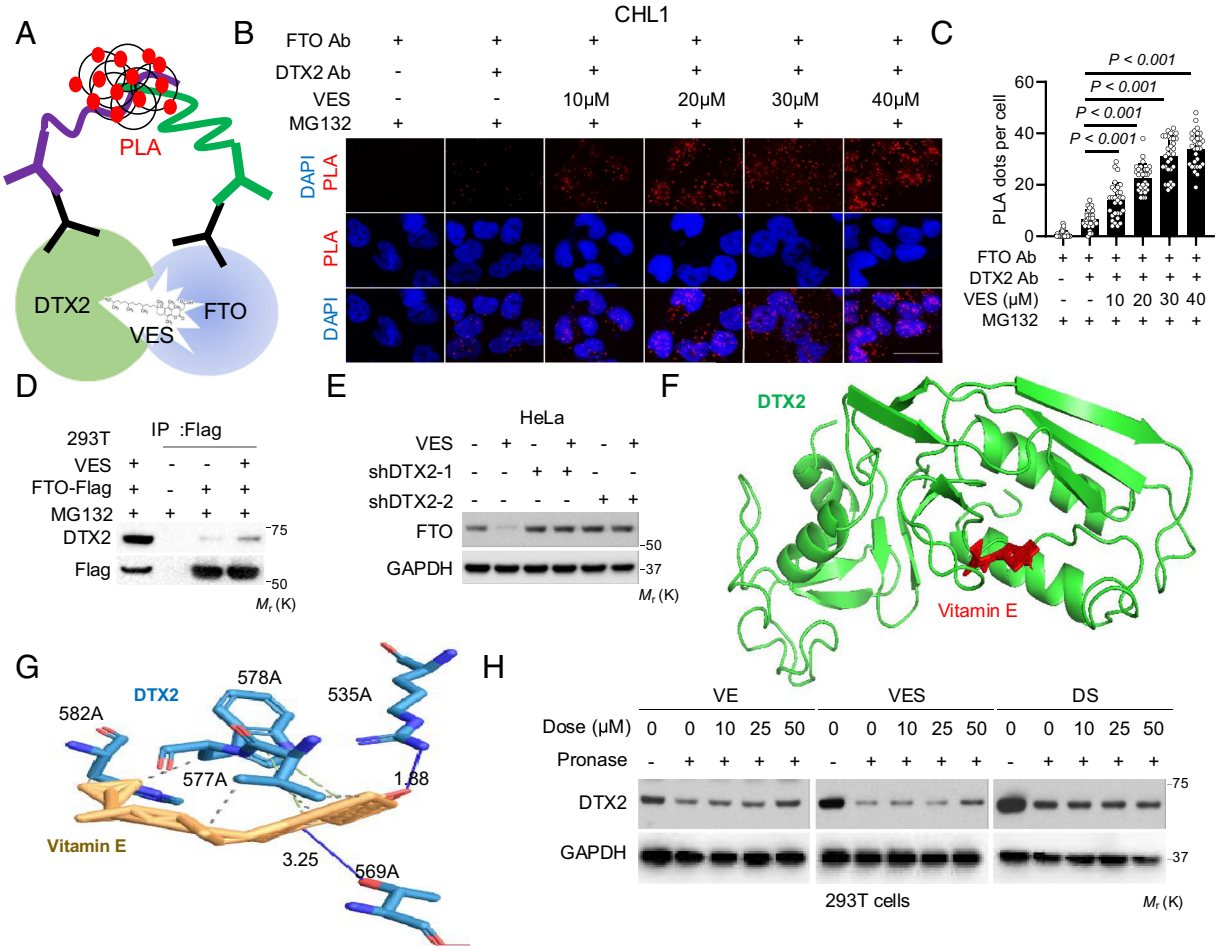

Fig. 3. VES induces FTO protein degradation via DTX2. (*A*) Schematic illustration of the in situ proximity ligation assay (PLA). (*B*) Immunofluorescence analysis of the PLA of the interaction between DTX2 and FTO in CHL1 cells. (Scale bar, 100 μm.) (*C*) Quantification of the number of PLA red dots per cell in *B* (n = 30 cells from three biologically independent replicates). (*D*) Co-IP analysis of FTO binding with DTX2 in 293T cells transfected with FTO-Flag and treated with or without VES (25 μM, 12 h) with MG132 (10 μM) for 6 h. (*E*) Immunoblot analysis of FTO in HeLa cells with or without DTX2 knockdown and treated with or without VES (25 μM, 72 h). (*F*) Molecular docking showing the interaction of DTX2 with vitamin *E*. (*G*) Diagram for vitamin E binding with DTX2. (*H*) Immunoblot analysis of DTX2 and GAPDH from DARTS assay in 293T cells treated with VES, VE, and DS. Error bars are shown as mean ± SD (*C*). *P*-values are from two-tailed unpaired *t* tests (*C*).

as a molecular glue degrader for FTO via enhancing the FTO–DTX2 interaction.

UFD1 Is Required for VES-Induced FTO Protein Degradation. To determine the detailed molecular mechanism in VES-induced FTO degradation, we performed a mass spectrometry analysis of FTO-interacting proteins modulated by VES (*SI Appendix*, Table S1). We found that VES drastically increases the interaction of FTO with Ubiquitin Fusion Degradation Protein 1 (UFD1) (Fig. 4*A*). UFD1 is a critical factor for recognizing ubiquitinated proteins, leading to their ultimate degradation (53, 54). Analysis of TCGA data showed that UFD1 expression is negatively associated with FTO expression in cancer (*SI Appendix*, Fig. S7 *A* and *B*). Moreover, UFD1 knockdown increased FTO protein level (*SI Appendix*, Fig. S7 *C* and *D*), whereas UFD1 overexpression decreased it (*SI Appendix*, Fig. S7 *E* and *F*). Consistently, UFD1 overexpression decreased the level of WT FTO but not the K162R mutant (Fig. 4*B*). Furthermore, UFD1 overexpression clearly decreased FTO protein stability, whereas UFD1 knockdown increased it (Fig. 4 *C*–*F*). Co-IP analysis showed that UFD1 binds with FTO (*SI Appendix*, Fig. S7*G*). VES increased UFD1 binding with WT FTO, but not the K162R mutant (Fig. 4 *G* and *H* and *SI Appendix*, Fig. S7*H*). Additionally, UFD1 knockdown reversed the effect of VES on FTO downregulation (Fig. 4*I*). The combination of DTX2 overexpression and UFD1 overexpression showed an additive effect on FTO downregulation as compared with overexpression of each factor alone (Fig. 4*J*), while overexpression of either DTX2 or UFD1 did not affect the protein level of other m^6A regulators, including the methyltransferase proteins METTL3 and METTL14 (*SI Appendix*, Fig. S7 *I* and *J*), establishing FTO as a specific target for DTX2 and UFD1. However, DARTS and CETSA analysis showed that VES does not bind to UFD1 (Fig. 4 *K* and *L* and *SI Appendix*, Fig. S7*K*). These results demonstrate that UFD1 binds to ubiquitinated FTO and is required for VES-induced FTO protein degradation (Fig. 4*M*).

To determine whether chronic VES treatment protects FTO from VES-induced degradation, we treated MEL624 cells with VES (10 μM) for 7 wk. Chronic VES treatment resulted in a slight decrease in FTO protein level and cell proliferation (*SI Appendix*, Fig. S7 *L* and *M*), while it did not affect the levels of either UFD1 or DTX2 (*SI Appendix*, Fig. S7*L*). However, when we treated the cells with 10 μM VES for 72 h, we found that chronic VES-treated cells showed resistance to VES-induced FTO downregulation (*SI Appendix*, Fig. S7 *L* and *M*). Future investigation is warranted to determine whether the resistance is caused by VES-induced genetic mutations, clonal selections, or epigenetic alterations that prevents FTO downregulation.

Effect of Targeting FTO Degradation in Tumor Growth and Response to Immunotherapy. Next, we investigated whether DTX2 and UFD1 play important roles in tumorigenesis. Indeed, DTX2 overexpression or UFD1 overexpression decreased cell proliferation in vitro (*SI Appendix*, Fig. S8 *A* and *B*). While overexpression of WT FTO increased cell proliferation, overexpression of WT DTX2, but not mutant DTX2, reversed the effect of WT FTO overexpression (Fig. 5*A* and *SI Appendix*, Fig. S8*C*). Moreover, overexpression of DTX2 or UFD1 decreased tumor growth (Fig. 5 *B* and *C* and *SI Appendix*, Fig. S8 *D* and *E*). Cells with FTO knockout showed reduced sensitivity to overexpression of either DTX2 or UFD1 (Fig. 5*D* and *SI Appendix*, Fig. S8*F*), suggesting that the effect of DTX2 and UFD1 is at least in part dependent on FTO. TCGA data analysis showed that mimicking FTO low expression, DTX2 high expression, or UFD1 high expression was associated with better survival for anti-PD-L1 immunotherapy (Fig. 5 *E*–*G*). Mimicking the effect of genetic FTO inhibition shown previously (37), VES sensitized melanoma cells to IFNγ-mediated toxicity (*SI Appendix*, Fig. S8*G*). Consistently, VES sensitized B16F10 tumors to anti-PD-1 immunotherapy (Fig. 5 *H* and *I*). Moreover, DTX2 expression was reduced in melanoma as compared with normal tissues, while FTO expression was increased (Fig. 5 *J* and *K*). As VES has been shown to induce apoptosis in cancer cells in vitro (46–49, 51), we assessed the effect of VES on tumor cell apoptosis in vivo in mice. However, we failed to detect increased apoptosis in VES-treated tumors in our mouse model (*SI Appendix*, Fig. S8 *H*–*K*), possibly due to the clearance of apoptotic cells in vivo or the VES dose used. Taken together, these data demonstrate that targeting FTO protein degradation suppresses tumorigenesis and enhances tumor response to immunotherapy.

VES Increased T Cell–Mediated Cytotoxicity by Targeting FTO. We next investigated the mechanism by which VES suppresses tumorigenesis and sensitizes tumors to immunotherapy. In addition to melanoma cells, we found that VES down-regulates FTO in MC38 cells (*SI Appendix*, Fig. S9*A*). When we used flow cytometry analysis to analyze the effect of VES on immune cell profiles in tumors (*SI Appendix*, Fig. S9*B*), we found that VES significantly increased the percentage of $CD8^+$ T cells and decreased the percentage of $CD206^+$ M2-like tumor-associated macrophages (TAM) (Fig. 6 *A*–*E*). Moreover, VES increased the percentage of $TNF\alpha^+$ and $IFN\gamma^+$ $CD8^+$ T cells and decreased $PD1^+$ $CD8^+$ T cells (Fig. 6 *F*–*H*). To determine the functional significance of $CD8^+$ T cells and $CD206^+$ TAMs, we treated mice with anti-CD8 and anti-G-CSF1R antibodies to deplete these cells. Depletion of $CD8^+$ T cells partially reversed the effect of VES, while depletion of TAMs had no effect (Fig. 6*I* and *SI Appendix*, Fig. S9 *C*–*F*).

We next assessed the potential role of VES's effect on the function of T cells. VES had no effect on the FTO protein level in activated human T cells (Fig. S9*G*). We noticed that FTO protein level is much lower in activated human T cells than MEL624 cells (*SI Appendix*, Fig. S9*H*). Next, we questioned whether VES affects T cell toxicity by regulating FTO in melanoma cells. Both supernatants from VES-treated MEL624 cells and a VES-pretreated coculture of MEL624 and T cells significantly increased the percentage of $CD8^+$ T cells in $CD3^+$ T cells (Fig. 6 *J* and *K*). Next, we hypothesized that VES induces T cell–mediated killing of tumor cells. Using a coculture system with human T cells and GFP-labeled human melanoma cells (Fig. 6*L*), we found that VES sensitized melanoma cells to T cell–mediated killing in an FTO-dependent manner (Fig. 6 *M* and *N* and *SI Appendix*, Fig. S9*I*). Similar to VES, DTX2 overexpression in melanoma cells sensitized tumor cells to T cell–mediated killing (Fig. 6*O*). These findings demonstrate that VES enhances T cell toxicity via targeting tumor-intrinsic FTO.

FTO Inhibition Enhances T Cell–Mediated Cytotoxicity by Targeting LIF. Next, we investigated the mechanism by which FTO regulates antitumor immunity. We first determined the common pathways affected by VES and FTO knockdown using RNA-seq analysis. Pathway analysis of VES's effect and reanalysis of our previous data (GSE112902) showed that both FTO knockdown and VES increased the activation of the JAK-STAT pathway and the cytokine receptor interaction pathway (Fig. 7*A* and *SI Appendix*, Fig. S10 *A*–*C*). We hypothesized that the cytokine(s) plays an important role in regulating T cell toxicity by FTO inhibition. We then focused on the JAK-STAT pathway and found that both FTO knockdown and VES up-regulated the expression of CDKN1A, IL11, IL24, LIF (Leukemia inhibitory factor), MCL1, and PIM1 (Fig. 7*B* and *SI Appendix*, S10*D*).

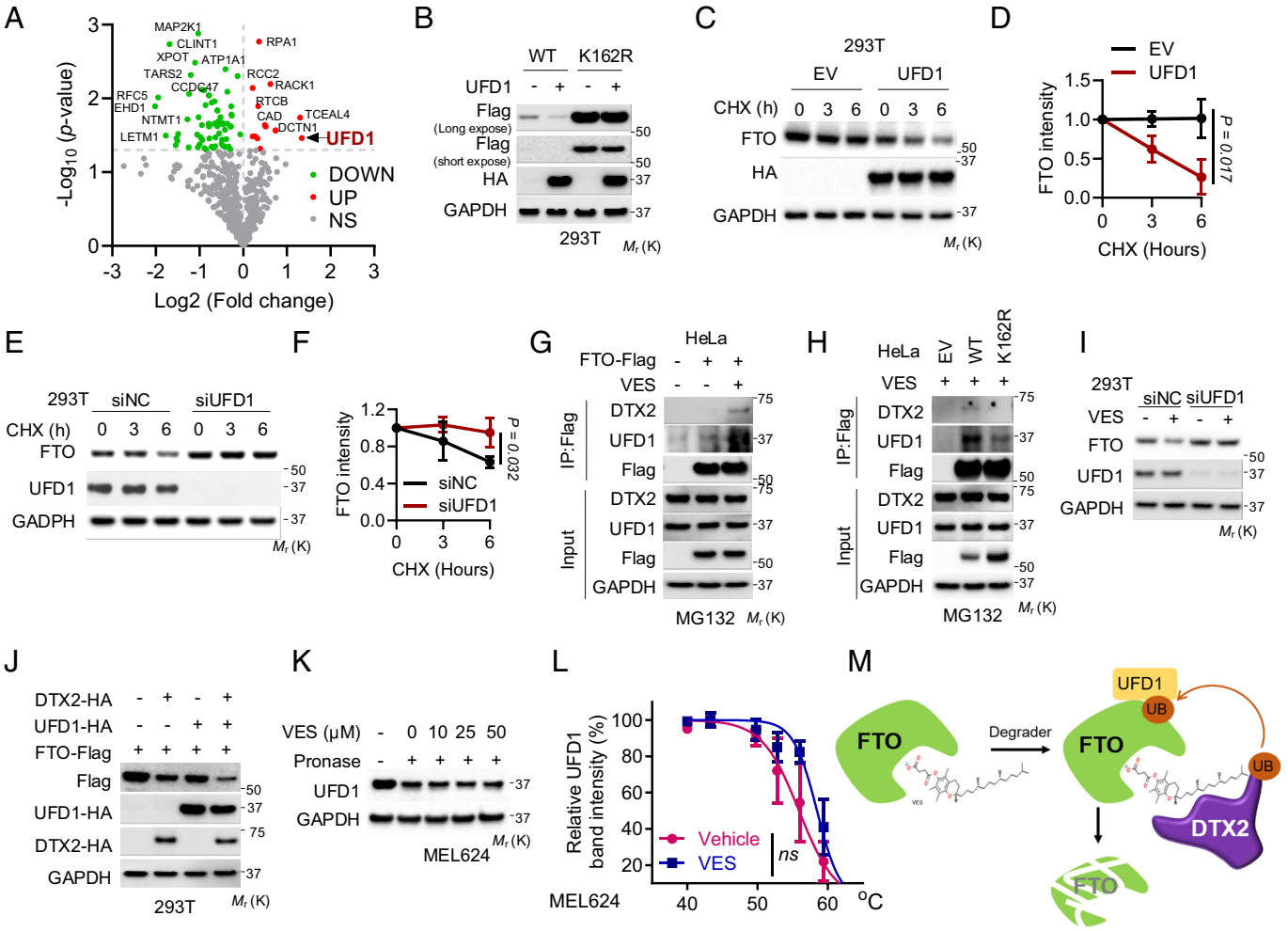

Fig. 4. UFD1 is required for VES-induced FTO protein degradation. (*A*) Volcano plot of FTO-interacting proteins in MEL624 cells from Co-IP followed by mass spectrometry analysis. (*B*) Immunoblot analysis of WT FTO, K162R FTO, and UFD1 in 293T cells transfected with or without FTO WT-Flag, FTO K162R-Flag, and UFD1-HA. (*C*) Immunoblot analysis of FTO in 293T cells transfected with or without UFD1 and treated with cycloheximide (CHX, 100 μg/ml) over a time course. (*D*) Quantification of *C* (n =3). (*E*) Immunoblot analysis of FTO in 293T cells with or without UFD1 knockdown treated with cycloheximide (CHX, 100 μg/ml) over a time course. (*F*) Quantification of E (n =3). (*G*) Co-IP assay showing the binding of FTO with DTX2 and UFD1 in HeLa cells transfected with FTO-Flag treated with or without VES (25 μM, 12 h) with MG132 (10 μM) for 6 h. (*H*) Co-IP assay showing the binding of FTO or FTO K162 with DTX2 or UFD1 in HeLa cells transfected with FTO WT and FTO K162R and treated with VES (25 μM, 12 h) with MG132 (10 μM) for 6 h. (*I*) Immunoblot analysis of FTO and UFD1 in 293T cells with or without UFD1 knockdown and treated with or without VES (10 μM, 72 h). (*J*) Immunoblot analysis of FTO, UFD1, and DTX2 in 293T cells with FTO-Flag overexpression and with or without overexpression of DTX2 and UFD1. (*K*) Immunoblot analysis of UFD1 and GAPDH from DARTS assay in MEL624 cells treated with or without VES. (*L*) Thermal shift curves of UFD1 from CETSA in MEL624 cells treated with or without VES (10 μM) (n = 3). (*M*) Schematic summary of VES-induced FTO protein degradation. Error bars are shown as mean ± SD (*D*, *F*, and *L*). *P*-values are from two-tailed unpaired *t* tests (*D*, *F*, and *L*).

Our previous m^{6}A-seq analysis (GSE112902) showed that FTO knockdown drastically increases m^{6}A enrichment across the LIF transcript, as well as in other genes (Fig. 7*C* and *SI Appendix*, Fig. S10 *E–I*). m^{6}A qPCR analysis validated the increased m^{6}A enrichment in LIF, IL24, and PIM1, but not in IL11, MCL1, or CDKN1A (Fig. 7*D*). Further analysis showed that either VES or FTO knockdown increased the mRNA stability of LIF, but not IL11 or IL24 consistently (Fig. 7*E* and *SI Appendix*, Fig. S11 *A–I*). Moreover, FTO overexpression decreased LIF mRNA stability (*SI Appendix*, Fig. S11*J*), suggesting that possible m^{6}A readers may be IGF2BP1-3, a group of m^{6}A readers that stabilize m^{6}A-modified transcripts (55). Indeed, knockdown of IGF2BP1, IGF2BP2, and IGF2BP3 decreased the stability of LIF mRNA (Fig. 7*F* and *SI Appendix*, Fig. S11*K*). FTO overexpression also decreased LIF mRNA levels, which was reversed by DTX2 overexpression (Fig. 7*G*). Indeed, LIF expression is negatively correlated with FTO expression in human melanomas and melanoma cell lines (Fig. 7*H* and *SI Appendix*, Fig. S12*A*). Moreover, LIF expression was decreased in melanoma (*SI Appendix*, Fig. S12*B*). Furthermore, high LIF expression was correlated with increased survival in melanoma (*SI Appendix*, Fig. S12*C*). These data suggest that LIF is a target for FTO-mediated m^{6}A mRNA demethylation.

Based on these findings, we hypothesized that LIF plays an important role in FTO's regulation of T cell cytotoxicity, as LIF is a secreted factor that can regulate tumor microenvironment (56–58). We found that LIF overexpression significantly decreased cell proliferation in vitro (Fig. 7 *I* and *J*). High expression of LIF or PIM1 was significantly associated with improved response to anti-PD-1 therapy in melanoma patients (Fig. 7*K* and *SI Appendix*, Fig. S12 *D–H*). To determine whether FTO inhibition enhances T cell cytotoxicity through regulating LIF, we assessed the effect of LIF overexpression in melanoma cells on T cell toxicity. We confirmed that LIF expression was significantly decreased by FTO overexpression (Fig. 7*L*). Indeed, LIF overexpression sensitized tumor cells to T cell cytotoxicity, which was prevented by FTO overexpression (Fig. 7*M*). In addition, LIF overexpression significantly increased the percentage of CD8$^+$ T cells in CD3$^+$ T cells when T cells were cocultured with MEL624 cells (Fig. 7*N*). Taken

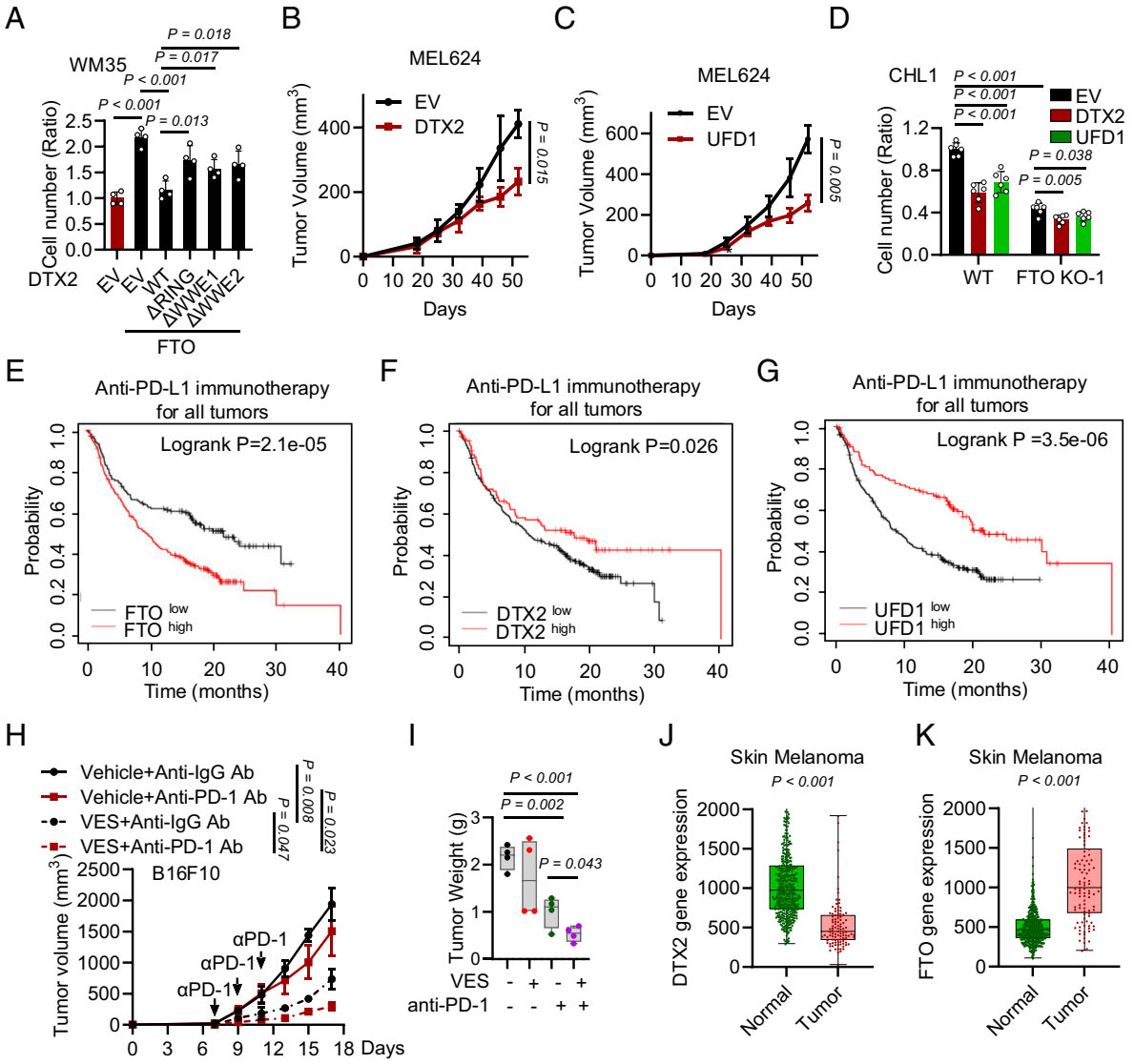

Fig. 5. Effect of targeting FTO degradation in tumor growth and response to immunotherapy. (*A*) Cell proliferation assay in WM35 cells with or without overexpression of FTO in combination with overexpression of WT DTX2 and DTX2 mutants (n = 4). (*B*) Tumor volume of MEL624 cells with or without DTX2 overexpression in nude mice (n = 5). (*C*) Tumor volume of MEL624 cells with or without UFD1 overexpression in nude mice (n = 5). (*D*) Cell proliferation assay in CHL1 cells with or without FTO deletion transfected with or without DTX2 and UFD1 (n = 6). (*E*) Overall survival of Pan-cancer patients with high FTO protein level (n = 295) and low FTO protein level (n = 164) following anti-PD-L1 immunotherapy. (*F*) Overall survival of Pan-cancer patients with high DTX2 protein level (n = 107) and low DTX2 protein level (n = 317) following anti-PD-L1 immunotherapy. (*G*) Overall survival of Pan-cancer patients with high UFD1 protein level (n = 126) and low UFD1 protein level (n = 298) following anti-PD-L1 immunotherapy. (*H*) Tumor volume of B16F10 cells injected in C57BL/6 mice treated with or without VES in combination with the anti-PD-1 antibody or the isotype control antibody (n = 4). (*I*) Tumor weight of *H*. (*J*) Boxplot showing gene expression of DTX2 in normal and skin melanoma tissue. (*K*) Boxplot showing gene expression of FTO in normal and skin melanoma tissue. Error bars are shown as mean ± SD (*A*, *D*, and *I*), ±SE (*B*, *C*, and *H*). *P*-values are from two-tailed unpaired *t* tests (*A*, *B*, *C*, *D*, *H*, *I*, *J*, and *K*).

together, our findings demonstrated that FTO in tumor cells reduces T cell cytotoxicity at least in part through m^{6}A demethylation of LIF.

Discussion

FTO can be a critical tumor-promoting factor in many cancers (4, 8) and has become a promising target of interest in developing small-molecule inhibitors for anticancer therapies (13). Here, we identified DTX2 as an E3 ubiquitin ligase for FTO and found that UFD1 recognizes ubiquitinated FTO, leading to FTO degradation (*SI Appendix*, Fig. S13). We also show that VES acts as a dietary degrader for FTO, a mechanism distinct from other published small-molecule FTO inhibitors. We demonstrate that VES suppresses tumor growth, enhances antitumor immunity, and sensitizes tumors to immunotherapy in mouse tumor models. At the molecular level, genetic inhibition of FTO or VES increased m^{6}A methylation of the LIF gene and thus decreased LIF mRNA decay, which then sensitizes tumor cells to T cell–mediated killing.

As a widely used dietary supplement, VES is an esterized bioactive form of alpha-tocopherol, one of the eight vitamin E isomers (59, 60). The mechanism of action of vitamin E isoforms and derivatives has been assumed to be mainly due to its antioxidant function against oxidative damage. Among various forms of vitamin E isomers and derivatives, VES likely has both vitamin E-dependent and -independent functions (59, 60). Previous data showed that VES induces apoptosis in tumor cells (46–49, 51). We showed that VES-induced cell apoptosis in vitro is dose-dependent. Although we failed to detect apoptosis in tumors in vivo, apoptosis of tumor cells may contribute to VES-induced tumor suppression. In addition, our findings implicated that tumor-intrinsic immune response and T cell cytotoxicity also play critical roles in VES-induced tumor suppression, as VES increased

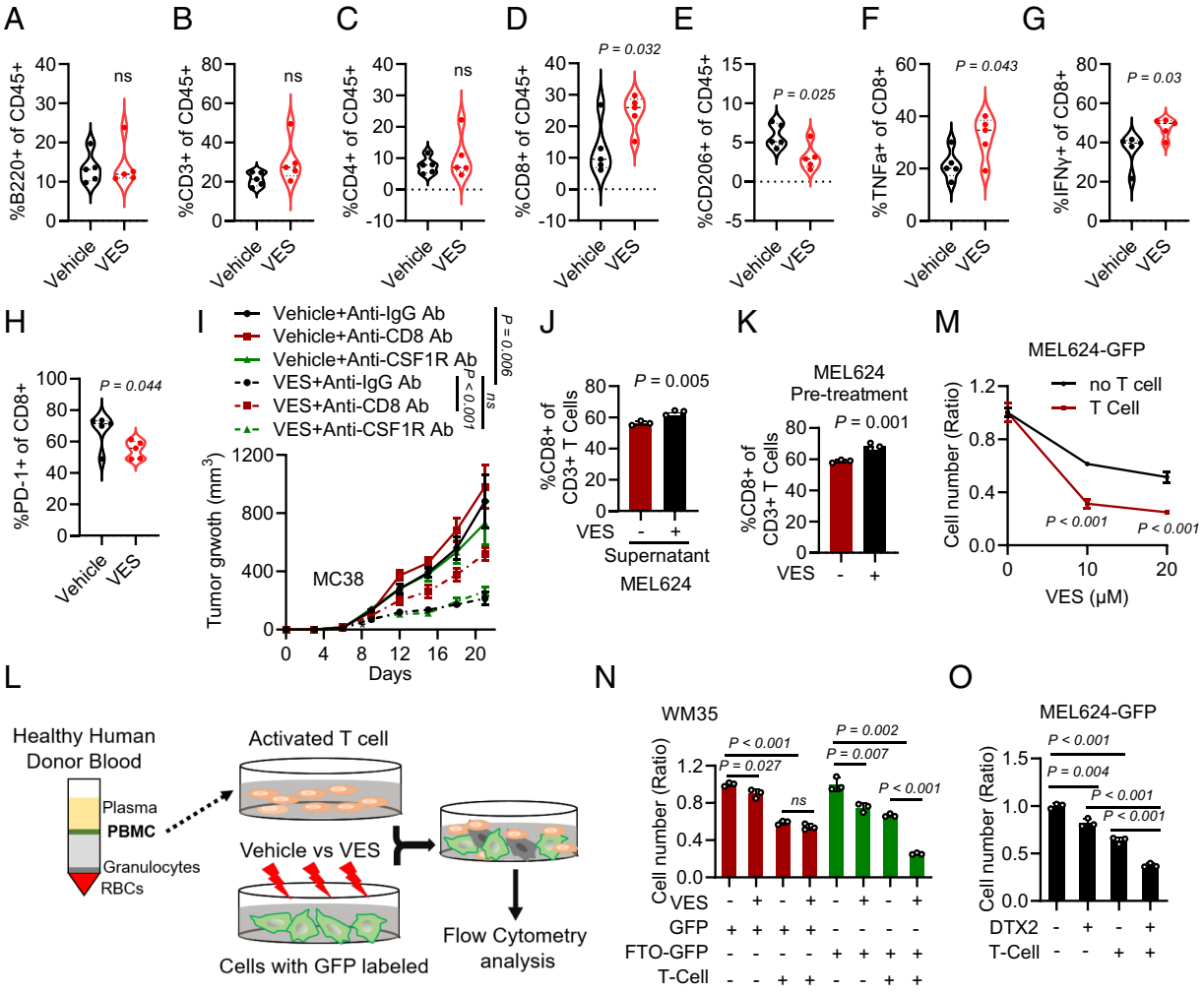

Fig. 6. VES increased T cell–mediated cytotoxicity by targeting FTO. (*A–E*) Quantification of mouse B220$^+$, CD3$^+$, CD4$^+$, CD8$^+$, and CD206$^+$ of CD45$^+$ cells in C57BL/6 mice bearing MC38 tumors upon treatment with vehicle and VES (n = 5). (*F–H*) Quantification of mouse TNFα$^+$, IFNγ$^+$, and PD-1$^+$ of CD8$^+$ T cells in C57BL/6 mice bearing MC38 tumors upon treatment with vehicle and VES (n = 5). (*I*) Tumor volume of MC38 tumors in C57BL/6 mice treated with or without VES in combination with the anti-CD8, anti-CSF1R, or isotype control antibody. (*J*) Quantification of CD8$^+$ of CD3$^+$ T cells in activated human T cells treated with or without supernatant from MEL624 cells treated with or without VES (n = 3). (*K*) Quantification of CD8$^+$ of CD3$^+$ T cells in activated human T cells cocultured with MEL624 and pretreated with or without VES (n = 3). (*L*) Schematic summary of the coculture assays for T cells and GFP-labeled human cancer cells. (*M*) Effect of VES on the sensitivity of MEL624-GFP cells to the cytotoxicity of T cells in vitro. MEL624 cells were pretreated with or without VES for 72 h (n = 3). (*N*) Effect of VES pretreatment (72 h) on the sensitivity of WM35 cells with or without FTO-GFP overexpression to the cytotoxicity of T cells in vitro (n = 3). (*O*) Effect of DTX2 overexpression in MEL624-GFP cells on the cytotoxicity of T cells in vitro (n = 3). Error bars are shown as mean ± SD (*A–H*, *J*, *K*, *M–O*), or ±SE (*I*). *P*-values are from two-tailed unpaired *t* tests (*A–K* and *M–O*).

intratumoral CD8$^+$ T cells and depletion of CD8$^+$ T cells partially reversed VES's effect on tumor suppression (Fig. 6 *D* and *I*). Future investigation is needed to elucidate detailed cellular mechanisms by which VES suppresses tumor growth.

Although some early preclinical studies indicated that VES had antitumor activities, but the specific molecular mechanisms are largely unknown. Our findings here revealed that unlike the previously published FTO inhibitors (CS1/2, FB23-2, etc.) that inhibits its activity, VES acts as an FTO degrader to target FTO for degradation by harnessing the cell's own destruction mechanisms. VES increased the FTO–DTX2 interaction and thus FTO ubiquitination and degradation, while it does not affect the protein abundance of other m^{6}A regulators and αKG-dependent enzymes (Fig. 2, S5O-P). VES seems to serve as a heterobifunctional protein degrader, with the succinate moiety binding with FTO and the VE moiety binding with DTX2, while VE or other VE derivatives, such as VEA, had no effect on FTO abundance (Figs. 2 and 3 and *SI Appendix*, Figs. S4 and S5). Our data also suggest that VES interacts with FTO, as detected from the effect of VES on FTO activity in the in vitro cell-free m^{6}A demethylase assay (Fig. 2*F*) and succinate has been shown to inhibit FTO demethylase activity (10, 50). Due to poor solubility of the recombinant full-length DTX2 protein, we were unable to obtain purified DTX2 protein to determine the direct binding of VES to FTO and DTX2 in detail. Future investigation is warranted to elucidate the structural and biophysical basis for the VES/FTO/DTX2 interaction with truncated DTX2 proteins to improve solubility. Those results implicate that VES acts as a specific molecular glue to induce FTO degradation via DTX2-mediated ubiquitination.

We identified LIF as a target of FTO-mediated m^{6}A RNA demethylation. LIF is a member of the IL-6 cytokine family and was identified as a crucial factor for mediating the self-renewal of mouse embryonic stem cells (ESCs) (61, 62). LIF expression and function is tissue-type dependent and can be either up-regulated or down-regulated in cancer tissues (63). LIF can act as either a tumor-suppressive or tumor-promoting factor (64–66). Mechanistically, the LIF receptor forms a heterodimer with gp130 upon LIF binding, which activates tyrosine kinase signaling pathways to induce gene transcription (64). In melanoma, we show that LIF is a target

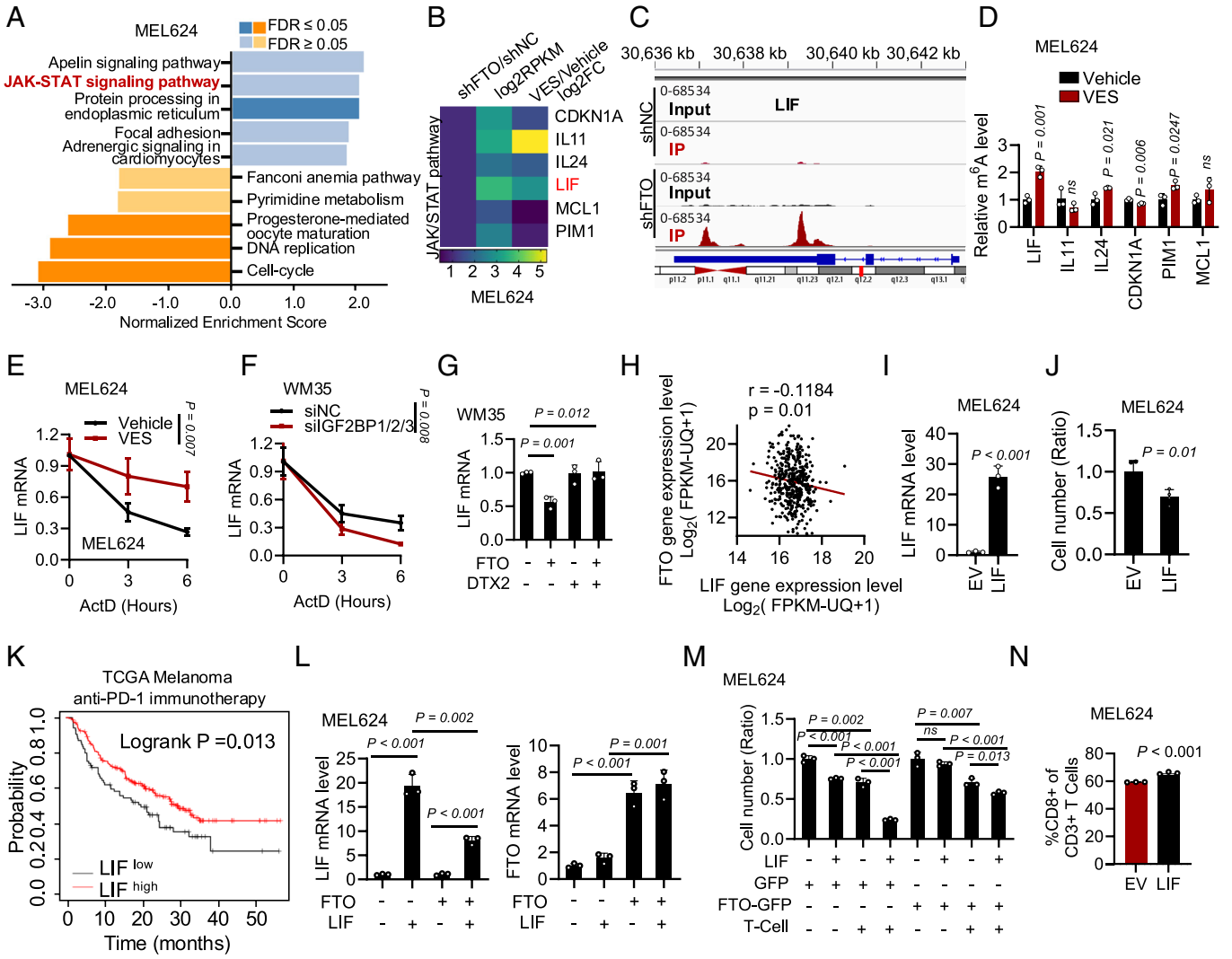

Fig. 7. FTO inhibition enhances T cell–mediated cytotoxicity by targeting LIF. (*A*) Pathway analysis of differentially expressed genes from RNA seq analysis of MEL624 cells with or without FTO knockdown (GSE112902). (*B*) Heatmap showing shared differentially expressed genes in the JAK-STAT signaling pathway by VES or FTO knockdown in MEL624 cells. (*C*) Distribution of m^{6}A peaks across the LIF transcript in MEL624 cells with or without FTO knockdown. (*D*) m^{6}A IP qPCR analysis of m^{6}A enrichment in the indicated gene transcripts in MEL624 cells treated with or without VES (n = 3). (*E*) qPCR analysis of LIF mRNA stability following treatment with actinomycin D (ActD, 2 μM) in MEL624 cells with or without VES treatment (n = 3). (*F*) qPCR analysis of LIF mRNA stability following treatment with actinomycin D (ActD, 2 μM) in WM35 cells with or without siRNA targeting IGF2BP1/2/3 without VES treatment (n = 3). (*G*) qPCR analysis of LIF mRNA level in WM35 cells with or without overexpression of FTO and DTX2 (n = 3). (*H*) Correlation plot of LIF mRNA level and FTO mRNA level in human melanoma tissue (n = 472). (*I*) qPCR analysis of LIF mRNA levels in MEL624 cells with or without LIF overexpression (n = 3). (*J*) Cell proliferation assay in MEL624 cells with or without LIF overexpression (n = 4). (*K*) Overall survival of melanoma patients with high LIF mRNA level (n = 233) and low LIF mRNA level (n = 92) following anti-PD-1 immunotherapy. (*L*) qPCR analysis of LIF and FTO mRNA level in MEL624 cells with or without FTO and LIF overexpression (n = 3). (*M*) Effect of LIF overexpression in MEL624 cells expressed with GFP or FTO-GFP on the cytotoxicity of T cells in vitro (n = 3). (*N*) Quantification of CD8$^+$ of CD3$^+$ T cells in activated human T cells cocultured with MEL624 with or without LIF overexpression (n = 3). Error bars are shown as mean ± SD (*D*–*G*, *I*, *J*, and *L*–*N*). Correlation coefficient r and *P*-value are from Pearson correlation analysis (*H*). *P*-values are from two-tailed unpaired *t* tests (*D*–*G*, *I*, *J*, and *L*–*N*).

for FTO-mediated m^{6}A demethylation and in part mediates the function of FTO in T cell toxicity. In addition to LIF, other FTO targets may also play important roles in antitumor immunity in different types of cancers, as FTO targets appear to be cell-type and context-dependent (4, 8). Previously LILRB4 has been shown to be a critical FTO target in leukemia cells (23). The role of FTO and its targets in regulating antitumor immunity in other types of tumors remains to be explored.

In summary, our findings not only elucidated the molecular mechanism that regulates FTO protein degradation but also revealed a dietary degrader for FTO to inhibit tumor growth and therapeutic resistance to immunotherapy. Our work on FTO degradation mechanisms and VES as an FTO degrader provide a mechanistic foundation and framework for the development of improved degraders for FTO with higher potency and specificity. In addition, as a widely used dietary supplement with known toxicology profiles, VES can potentially be developed into a therapeutic agent to mitigate immunotherapy resistance for patients with FTO-dependent cancers.

Materials and Methods

Mouse Tumorigenesis and Treatment, Cells, Cell Proliferation Assay, Coculture Assay for Human Melanoma Cells and Human T Cells, Tumor-Infiltrating Immune Cell Analysis, and Flow Cytometric Analysis. The Institutional Animal Care and Use Committee (IACUC) at the University of Chicago approved all of the animal procedures used in this study. Nude mice and C57BL/6 mice were utilized in the study. For xenograft experiments, tumor cells were injected subcutaneously into the right flanks of the mice. Antibodies and inhibitors were administered via intraperitoneal injection. The following cell lines were used: HaCaT, WM35, LLC, MC38, HeLa, HEK-293T, A375, MEL624, CHL-1, SK-MEL30, and B16F10. Cell proliferation was assessed using a Cell Counting Kit-8 (CCK-8). Human primary T cells were expanded in TexMACS™

GMP Medium and cocultured with VES-treated MEL624 or WM35 cells for 48 h. GFP+ cells were quantified using flow cytometry and analyzed with FlowJo V10 Software. Tumor tissues from tumor-bearing mice were digested to isolate immune cells, which were then stained with surface markers and intracellular cytokines for analysis. Cells were prepared for flow cytometry to assess immune profiles, following specific staining protocols. The gating strategy is detailed in *SI Appendix*, Fig. S12. Apoptotic cell death was evaluated using an Annexin V-FITC apoptosis detection kit and analyzed with a BD flow cytometer (FACS Calibur, LSR Fortessa, or LSRII, BD Biosciences).

Cloning, Plasmids, Lentiviral Infection, and siRNA Transfection. Domain deletions and point mutants were generated using the corresponding primers listed in *SI Appendix*, Table S3. Stable cell lines were created by infecting cells with lentiviral vectors. Cells were transfected with siRNA using PepMute™ siRNA Transfection Reagent (SignaGen).

Analysis of Protein and RNA Abundance, m^{6}A RNA Modification, 5hmC DNA Modification, Protein–Protein Interaction, Protein–RNA Interaction, Protein–VES Interaction, Mass Spectrometric Analysis, RNA Sequencing, Pathway Analysis, Human Database Analysis and Survival Analysis, and Molecular Docking. Protein abundance in cells or tissues was assessed using immunoblotting, immunofluorescence, ubiquitination assays, and flow cytometry. RNA abundance and stability were evaluated using qPCR analysis and RNA sequencing. m^{6}A RNA or 5hmC modifications were analyzed using dot blot or LC-MS/MS spectrometry. Protein–protein interactions were assessed by coimmunoprecipitation followed by immunoblotting, mass spectrometry, or in situ proximity ligation (PLA) assays. Protein–RNA interactions were evaluated using RNA immunoprecipitation (RIP) followed by qPCR analysis. The interaction between protein and VES was assessed using Drug Affinity Responsive Targets Stability (DARTS) assay, Cellular Thermal Shift Assay (CETSA), and RNA m^{6}A demethylation assay in a cell-free system. GO and KEGG pathway enrichment analyses were conducted using Metascape, while gene expression correlation and overall survival analyses utilized PINA v3.0, UCSC Xena, and KM Plot. GSEA and heatmaps of significant genes were generated using WebGestalt. VES ligands were created with Chemdraw and optimized using LigPrep in Schrödinger 2018. The X-ray structure of FTO (PDB code 4IE6) was used and Induced Fit docking was conducted with a 20 Å grid centered on the binding site, including key residues such as ARG316 and TYR295.

Data, Materials, and Software Availability. RNA seq data have been deposited in GEO [RNA sequencing data are accessible at the GEO repository, under accession number GSE250332 (67). All the software and packages used in this article are publicly available.

ACKNOWLEDGMENTS. We thank Dr. Ann Motten for a critical reading of the manuscript. We thank the Human Tissue Resource Center (HTRC, RRID:SCR_019199) for their assistance with histology and the Cytometry and Antibody Technology core facility (CAT, RRID: SCR_017760) for their assistance with flow cytometric analysis at The University of Chicago. We thank Dr. Norbert Fusenig for providing the HaCaT cells. This work was supported in part by NIH grants ES031693 (Y.-Y.H.), ES031534 (Y.-Y.H.), the University of Chicago Comprehensive Cancer Center (CA014599), CACHET (ES027792), and the University of Chicago Friends of Dermatology Endowment Fund. C.H. is an investigator of the HHMI.

Author affiliations: [a]Department of Medicine, Section of Dermatology, University of Chicago, Chicago, IL 60637; [b]Departments of Chemistry, Institute for Biophysical Dynamics, University of Chicago, Chicago, IL 60637; [c]Department of Biochemistry and Molecular Biology Institute for Biophysical Dynamics University of Chicago, Chicago, IL 60637; [d]Department of Medicine, Section of Hematology and Oncology, University of Chicago, Chicago, IL 60637; [e]Committee on Cancer Biology, University of Chicago, Chicago, IL 60637; [f]The College, University of Chicago, Chicago, IL 60637; [g]Department of Pediatrics, Section of Hematology/Oncology, University of Chicago, Chicago, IL 60637; and [h]HHMI, University of Chicago, Chicago, IL 60637

1. I. A. Roundtree, M. E. Evans, T. Pan, C. He, Dynamic RNA modifications in gene expression regulation. *Cell* **169**, 1187–1200 (2017).
2. B. S. Zhao, I. A. Roundtree, C. He, Post-transcriptional gene regulation by mRNA modifications. *Nat. Rev. Mol. Cell Biol.* **18**, 31–42 (2017).
3. S. Li, C. E. Mason, The pivotal regulatory landscape of RNA modifications. *Annu. Rev. Genomics Hum. Genet.* **15**, 127–150 (2014).
4. I. Barbieri, T. Kouzarides, Role of RNA modifications in cancer. *Nat. Rev. Cancer* **20**, 303–322 (2020).
5. M. Schapira, Structural chemistry of human RNA methyltransferases. *ACS Chem. Biol.* **11**, 575–582 (2016).
6. X. Jiang *et al.*, The role of m6A modification in the biological functions and diseases. *Signal Transduct. Target Ther.* **6**, 74 (2021).
7. N. Song *et al.*, The role of m6A RNA methylation in cancer: Implication for nature products anti-cancer research. *Front Pharmacol.* **13**, 933332 (2022).
8. H. Huang, H. Weng, J. Chen, m(6)A modification in coding and non-coding RNAs: Roles and therapeutic implications in cancer. *Cancer Cell* **37**, 270–288 (2020).
9. G. Jia *et al.*, N6-methyladenosine in nuclear RNA is a major substrate of the obesity-associated FTO. *Nat. Chem. Biol.* **7**, 885–887 (2011).
10. T. Gerken *et al.*, The obesity-associated FTO gene encodes a 2-oxoglutarate-dependent nucleic acid demethylase. *Science* **318**, 1469–1472 (2007).
11. M. A. Kurowski, A. S. Bhagwat, G. Papaj, J. M. Bujnicki, Phylogenomic identification of five new human homologs of the DNA repair enzyme AlkB. *BMC Genomics* **4**, 48 (2003).
12. X. Deng *et al.*, RNA N(6)-methyladenosine modification in cancers: Current status and perspectives. *Cell Res.* **28**, 507–517 (2018).
13. Y. Li, R. Su, X. Deng, Y. Chen, J. Chen, FTO in cancer: Functions, molecular mechanisms, and therapeutic implications. *Trends Cancer* **8**, 598–614 (2022).
14. B. Chen *et al.*, Development of cell-active N6-methyladenosine RNA demethylase FTO inhibitor. *J. Am. Chem. Soc.* **134**, 17963–17971 (2012).
15. G. Zheng *et al.*, Synthesis of a FTO inhibitor with anticonvulsant activity. *ACS Chem. Neurosci.* **5**, 658–665 (2014).
16. Y. Huang *et al.*, Meclofenamic acid selectively inhibits FTO demethylation of m6A over ALKBH5. *Nucleic Acids Res.* **43**, 373–384 (2015).
17. T. Wang *et al.*, Fluorescein derivatives as bifunctional molecules for the simultaneous inhibiting and labeling of FTO protein. *J. Am. Chem. Soc.* **137**, 13736–13739 (2015).
18. W. He *et al.*, Identification of a novel small-molecule binding site of the fat mass and obesity associated protein (FTO). *J. Med. Chem.* **58**, 7341–7348 (2015).
19. F. McMurray *et al.*, Pharmacological inhibition of FTO. *PLoS One* **10**, e0121829 (2015).
20. M. Padariya, U. Kalathiya, Structure-based design and evaluation of novel N-phenyl-1H-indol-2-amine derivatives for fat mass and obesity-associated (FTO) protein inhibition. *Comput. Biol. Chem.* **64**, 414–425 (2016).
21. R. Su *et al.*, R-2HG exhibits anti-tumor activity by targeting FTO/m(6)A/MYC/CEBPA signaling. *Cell* **172**, 90–105.e123 (2018).
22. Y. Huang *et al.*, Small-molecule targeting of oncogenic FTO demethylase in acute myeloid leukemia. *Cancer Cell* **35**, 677–691.e10 (2019).
23. R. Su *et al.*, Targeting FTO suppresses cancer stem cell maintenance and immune evasion. *Cancer Cell* **38**, 79–96.e11 (2020).
24. Q. Li *et al.*, Rhein inhibits AlkB repair enzymes and sensitizes cells to methylated DNA damage. *J. Biol. Chem.* **291**, 11083–11093 (2016).
25. Y. Liu *et al.*, Tumors exploit FTO-mediated regulation of glycolytic metabolism to evade immune surveillance. *Cell Metab.* **33**, 1221–1233.e11 (2021).
26. E. McShane, M. Selbach, Physiological functions of intracellular protein degradation. *Annu. Rev. Cell Dev. Biol.* **38**, 241–262 (2022).
27. D. Senft, J. Qi, Z. A. Ronai, Ubiquitin ligases in oncogenic transformation and cancer therapy. *Nat. Rev. Cancer* **18**, 69–88 (2018).
28. D. A. Cruz Walma, Z. Chen, A. N. Bullock, K. M. Yamada, Ubiquitin ligases: Guardians of mammalian development. *Nat. Rev. Mol. Cell Biol.* **23**, 350–367 (2022).
29. D. Chirnomas, K. R. Hornberger, C. M. Crews, Protein degraders enter the clinic–a new approach to cancer therapy. *Nat. Rev. Clin. Oncol.* **20**, 265–278 (2023).
30. B. Dale *et al.*, Advancing targeted protein degradation for cancer therapy. *Nat. Rev. Cancer* **21**, 638–654 (2021).
31. M. Jan, A. S. Sperling, B. L. Ebert, Cancer therapies based on targeted protein degradation–lessons learned with lenalidomide. *Nat. Rev. Clin. Oncol.* **18**, 401–417 (2021).
32. Y. H. Cui *et al.*, Autophagy of the m(6)A mRNA demethylase FTO is impaired by low-level arsenic exposure to promote tumorigenesis. *Nat. Commun.* **12**, 2183 (2021).
33. Y. Du *et al.*, PINA 3.0: Mining cancer interactome. *Nucleic Acids Res.* **49**, D1351–D1357 (2021).
34. M. J. Cowley *et al.*, PINA v2.0: mining interactome modules. *Nucleic Acids Res.* **40**, D862–D865 (2012).
35. J. Wu *et al.*, Integrated network analysis platform for protein-protein interactions. *Nat. Methods* **6**, 75–77 (2009).
36. L. Wang, X. Sun, J. He, Z. Liu, FunctiOns and molecular mechanisms of deltex family ubiquitin E3 ligases in development and disease. *Front Cell Dev. Biol.* **9**, 706997 (2021).
37. S. Yang *et al.*, m(6)A mRNA demethylase FTO regulates melanoma tumorigenicity and response to anti-PD-1 blockade. *Nat. Commun.* **10**, 2782 (2019).
38. R. Revici, S. Hosseini-Alghaderi, F. Haslam, R. Whiteford, M. Baron, E3 ubiquitin ligase regulators of notch receptor endocytosis: From flies to humans. *Biomolecules* **12**, 224 (2022).
39. I. Dikic, S. Wakatsuki, K. J. Walters, Ubiquitin-binding domains–from structures to functions. *Nat. Rev. Mol. Cell Biol.* **10**, 659–671 (2009).
40. Z. A. Wang, P. A. Cole, The chemical biology of reversible lysine post-translational modifications. *Cell Chem. Biol.* **27**, 953–969 (2020).
41. R. Kumar *et al.*, Comprehensive mutations analyses of FTO (fat mass and obesity-associated gene) and their effects on FTO's substrate binding implicated in obesity. *Front Nutr.* **9**, 852944 (2022).
42. M. H. Glickman, A. Ciechanover, The ubiquitin-proteasome proteolytic pathway: Destruction for the sake of construction. *Physiol. Rev.* **82**, 373–428 (2002).
43. X. Yuan *et al.*, Vitamin E enhances cancer immunotherapy by reinvigorating dendritic cells via targeting checkpoint SHP1. *Cancer Discov.* **12**, 1742–1759 (2022).
44. R. A. Luchtel *et al.*, High-dose ascorbic acid synergizes with anti-PD1 in a lymphoma mouse model. *Proc. Natl. Acad. Sci. U.S.A.* **117**, 1666–1677 (2020).

45. A. Magri *et al.*, High-dose vitamin C enhances cancer immunotherapy. *Sci. Transl. Med.* **12**, eaay8707 (2020).
46. D. Patacsil *et al.*, Vitamin E succinate inhibits survivin and induces apoptosis in pancreatic cancer cells. *Genes. Nutr.* **7**, 83–89 (2012).
47. J. M. Turley *et al.*, Vitamin E succinate inhibits proliferation of BT-20 human breast cancer cells: Increased binding of cyclin A negatively regulates E2F transactivation activity. *Cancer Res.* **57**, 2668–2675 (1997).
48. J. Ni *et al.*, Vitamin E succinate inhibits human prostate cancer cell growth via modulating cell cycle regulatory machinery. *Biochem. Biophys. Res. Commun.* **300**, 357–363 (2003).
49. K. Israel, W. Yu, B. G. Sanders, K. Kline, Vitamin E succinate induces apoptosis in human prostate cancer cells: Role for Fas in vitamin E succinate-triggered apoptosis. *Nutr. Cancer* **36**, 90–100 (2000).
50. J. D. W. Toh *et al.*, A strategy based on nucleotide specificity leads to a subfamily-selective and cell-active inhibitor of N(6)-methyladenosine demethylase FTO. *Chem. Sci.* **6**, 112–122 (2015).
51. J. Neuzil, T. Weber, N. Gellert, C. Weber, Selective cancer cell killing by alpha-tocopheryl succinate. *Br. J. Cancer* **84**, 87–89 (2001).
52. Y. Fang *et al.*, Targeted protein degrader development for cancer: Advances, challenges, and opportunities. *Trends Pharmacol. Sci.* **44**, 303–317 (2023).
53. Y. Ye, H. H. Meyer, T. A. Rapoport, Function of the p97-Ufd1-Npl4 complex in retrotranslocation from the ER to the cytosol: Dual recognition of nonubiquitinated polypeptide segments and polyubiquitin chains. *J. Cell Biol.* **162**, 71–84 (2003).
54. E. E. Blythe, K. C. Olson, V. Chau, R. J. Deshaies, Ubiquitin- and ATP-dependent unfoldase activity of P97/VCP*NPLOC4*UFD1L is enhanced by a mutation that causes multisystem proteinopathy. *Proc. Natl. Acad. Sci. U.S.A.* **114**, E4380–E4388 (2017).
55. H. Huang *et al.*, Publisher correction: Recognition of RNA N(6)-methyladenosine by IGF2BP proteins enhances mRNA stability and translation. *Nat. Cell Biol.* **22**, 1288 (2020).
56. M. Pascual-Garcia *et al.*, LIF regulates CXCL9 in tumor-associated macrophages and prevents CD8(+) T cell tumor-infiltration impairing anti-PD1 therapy. *Nat. Commun.* **10**, 2416 (2019).
57. C. L. Stewart *et al.*, Blastocyst implantation depends on maternal expression of leukaemia inhibitory factor. *Nature* **359**, 76–79 (1992).
58. J. Albrengues *et al.*, LIF mediates proinvasive activation of stromal fibroblasts in cancer. *Cell Rep.* **7**, 1664–1678 (2014).
59. J. Neuzil, Vitamin E succinate and cancer treatment: A vitamin E prototype for selective antitumour activity. *Br. J. Cancer* **89**, 1822–1826 (2003).
60. K. N. Prasad, B. Kumar, X. D. Yan, A. J. Hanson, W. C. Cole, Alpha-tocopheryl succinate, the most effective form of vitamin E for adjuvant cancer treatment: A review. *J. Am. Coll. Nutr.* **22**, 108–117 (2003).
61. S. Kuphal, S. Wallner, A. K. Bosserhoff, Impact of LIF (leukemia inhibitory factor) expression in malignant melanoma. *Exp. Mol. Pathol.* **95**, 156–165 (2013).
62. E. A. Casanova *et al.*, Pramel7 mediates LIF/STAT3-dependent self-renewal in embryonic stem cells. *Stem. Cells* **29**, 474–485 (2011).
63. M. M. Jorgensen, P. de la Puente, Leukemia inhibitory factor: An important cytokine in pathologies and cancer. *Biomolecules* **12**, 217 (2022).
64. N. A. Nicola, J. J. Babon, Leukemia inhibitory factor (LIF). *Cytokine Growth Factor Rev.* **26**, 533–544 (2015).
65. S. Penuelas *et al.*, TGF-beta increases glioma-initiating cell self-renewal through the induction of LIF in human glioblastoma. *Cancer Cell* **15**, 315–327 (2009).
66. S. C. Liu *et al.*, Leukemia inhibitory factor promotes nasopharyngeal carcinoma progression and radioresistance. *J. Clin. Invest.* **123**, 5269–5283 (2013).
67. E. Wilkinson, Y. H. Cui, Data from "FTO degradation targeting enhances anti-tumor immunity." Gene Expression Omnibus. https://www.ncbi.nlm.nih.gov/geo/query/acc.cgi?acc=GSE250332. Deposited 15 December 2023.